Enhancement of the Electrical Properties of Graphene Grown by Chemical Vapor Deposition via Controlling the Effects of Polymer Residue

Ji Won Suk,[†] Wi Hyoung Lee,[†,‡] Jongho Lee,[§] Harry Chou,[†] Richard D. Piner,[†] Yufeng Hao,[†] Deji Akinwande,[§] and Rodney S. Ruoff*[,†]

[†]Department of Mechanical Engineering and the Materials Science and Engineering Program, The University of Texas at Austin, Austin, Texas, 78712, United States

[‡]Department of Organic and Nano System Engineering, Konkuk University, Seoul, 143-701, South Korea

[§]Department of Electrical and Computer Engineering, Microelectronics Research Center, The University of Texas at Austin, Austin, Texas, 78758, United States

Ⓢ Supporting Information

ABSTRACT: Residual polymer (here, poly(methyl methacrylate), PMMA) left on graphene from transfer from metals or device fabrication processes affects its electrical and thermal properties. We have found that the amount of polymer residue left after the transfer of chemical vapor deposited (CVD) graphene varies depending on the initial concentration of the polymer solution, and this residue influences the electrical performance of graphene field-effect transistors fabricated on SiO_2/Si. A PMMA solution with lower concentration gave less residue after exposure to acetone, resulting in less p-type doping in graphene and higher charge carrier mobility. The electrical properties of the weakly p-doped graphene could be further enhanced by exposure to formamide with the Dirac point at nearly zero gate voltage and a more than 50% increase of the room-temperature charge carrier mobility in air. This can be attributed to electron donation to graphene by the $-NH_2$ functional group in formamide that is absorbed in the polymer residue. This work provides a route to enhancing the electrical properties of CVD-grown graphene even when it has a thin polymer coating.

KEYWORDS: Graphene, polymer (PMMA) residue, electrical properties, graphene transfer, field-effect transistor, formamide
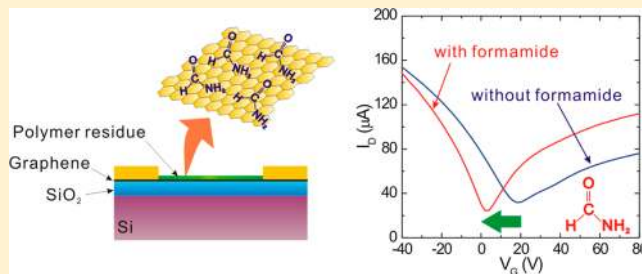
G raphene has attracted tremendous interest due to its electronic properties that make it a promising candidate for nanoelectronics.[1−4] Chemical vapor deposition (CVD) on copper has yielded large-area monolayer graphene for various device applications.[5] However, to fabricate graphene-based electronic devices, graphene grown on metal substrates such as copper needs to be transferred onto an insulating substrate such as SiO_2 or hexagonal boron nitride. A now common method for transferring monolayer graphene to another substrate is to use a polymer such as poly(methyl methacrylate) (PMMA) as a support film, followed by dissolution of the Cu foil, transfer to the desired substrate, and then (attempted) removal of all polymer such as with solvents.[6,7] However, this transfer process and also device fabrication processes such as lithography, inevitably contaminates the graphene surface with polymer residues present, for example, as a 1−2 nm thick continuous film even after the polymer support film is "removed" with solvents such as acetone.[8]

Graphene's properties are strongly influenced by its immediate environment, including any residue polymer film, and any adsorbed molecules.[9−11] Physisorbed molecules on graphene surfaces impact the electrical[12−14] and thermal[15]

properties by doping or providing scattering sites, which effectively alters the electronic structure of graphene or reduces the mean free path of charge carriers or phonons. For example, a thin PMMA layer left on graphene is reported to cause p-type doping in graphene field-effect transistors (GFETs) and to lower charge carrier mobility.[16] The wide range of reported charge carrier mobilities is likely due both to differences in the quality of the as-grown graphene as well as to residues from transfer and/or device fabrication.[17,18]

Heating graphene at 300−400 °C in Ar/H_2[8,14,19] including in ultrahigh vacuum[16] has been used to decompose the polymer residue(s), after which high-resolution transmission electron microscopy (TEM)[15] and scanning tunneling microscopy[8] could reveal its atomic structure. However, a systematic TEM study of PMMA decomposition on graphene has shown that thermal annealing cannot entirely remove the thin PMMA layer on graphene.[20] Furthermore, heating at such temperatures is
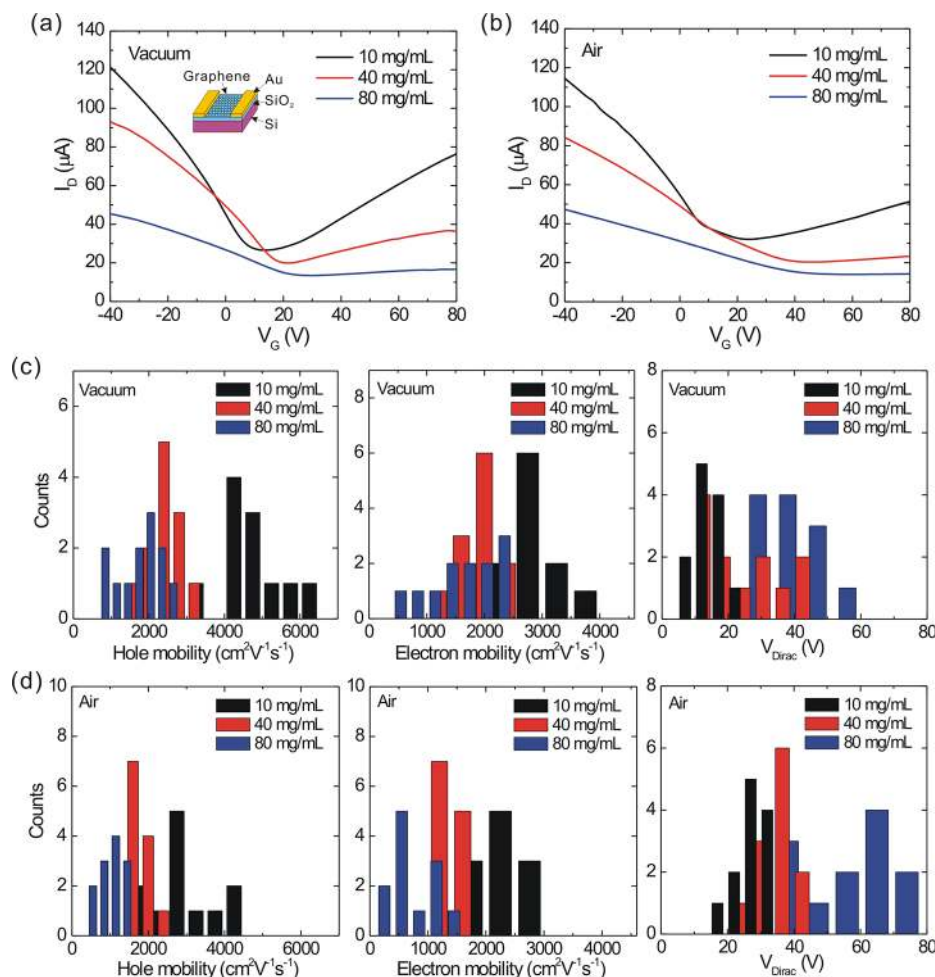
Figure 1. (a, b) Current−voltage (I_D−V_G) curves for the GFETs measured (a) in vacuum and (b) in air, as a function of the initial concentration of the PMMA solution. The inset shows the geometry of the GFET. (c, d) The hole/electron mobilities and Dirac point voltage (V_{Dirac}) for 12 GFETs measured (c) in vacuum and (d) in air.

reported to induce a strong interaction between graphene and the supporting SiO_2 substrate that intensifies the effects of charged impurities at the graphene−SiO_2 interface.[12] This causes GFETs to be highly p-doped with reduced carrier mobility,[14] which can be detected by the presence of a significant blue shift of Raman G and 2D peaks and a decreased integrated intensity ratio of the 2D band to the G band (I_{2D}/I_G).[21,22] Such high-temperature annealing is not suitable for plastic electronics where graphene can be used as a transparent conductive electrode,[23] and also as an active device component.[24−28] In addition to heat treatment in an oven or by conduction through a substrate, a current conducted through the graphene film was reported to remove contamination on the graphene surface by Joule heating.[29]

We report here the effect of polymer residue on the electrical properties of CVD-grown graphene as a function of the concentration of a solution of PMMA. This study includes GFET device fabrication and characterization, and surface characterization using X-ray photoelectron spectroscopy (XPS), Raman spectroscopy, and atomic force microscopy (AFM). Exposure of the GFETs to formamide showed dramatically enhanced electrical properties with the Dirac point at nearly zero gate voltage and increased charge carrier mobility.

To fabricate back-gated GFETs, monolayer graphene grown on copper by CVD[5] was transferred onto 285 nm thick SiO_2 on

highly doped Si (resistivity of 0.001−0.005 Ω·cm, Ultrasil corporation) using a PMMA-assisted transfer technique.[7] Three different PMMA concentrations (10, 40, and 80 mg/mL in chlorobenzene; M_w 996000, Sigma-Aldrich) were spin-coated on the graphene/copper piece with dimensions of about 1 cm × 1 cm at 4000 rpm, which generated ∼80 nm, ∼200 nm, and ∼700 nm thick PMMA films, respectively. The copper was etched with 0.1 M ammonium persulfate (ACS reagent grade, ≥98.0%, Sigma-Aldrich) by floating the PMMA/graphene/copper. After rinsing the PMMA/graphene with distilled water (by Barnstead MEGA-PURE 3A Water Still, Thermo Scientific) and transferring the PMMA/graphene films onto SiO_2/Si, the PMMA films were "removed" by immersing the samples in acetone (certified ACS grade, ≥99.5%, Fisher Scientific) for ∼24 h, and the acetone was exchanged three times. To avoid contamination from additional wet chemical processes such as photolithography, a shadow mask was used to thermally deposit Cr(5 nm)/Au(50 nm) for source and drain electrodes on the transferred graphene films.

Two-probe electrical measurements were carried out with a semiconductor device analyzer (model B1500, Agilent) at room temperature. The gate voltage was applied through the back side of the Si substrate, and the source−drain bias was constant at 0.01 V. The channel width (W) and length (L) were 300 and 50 μm, respectively. Figure 1a shows the representative
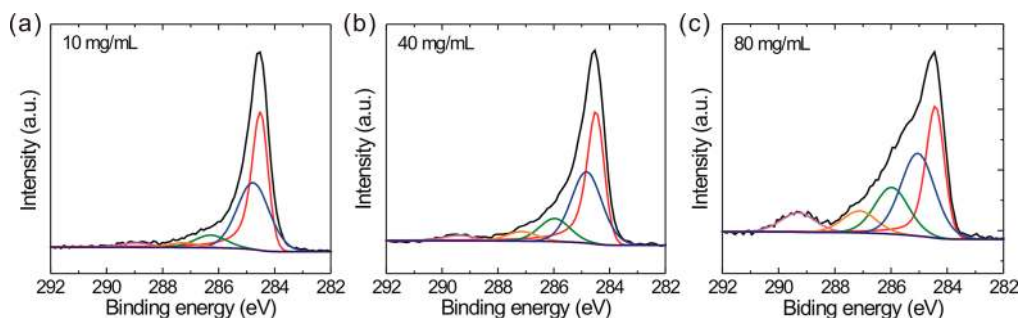
Figure 2. XPS C 1s spectra of the transferred graphene as a function of the initial concentration of the PMMA solution. The black line represents the measured XPS spectrum, and the five colored lines are deconvoluted peaks; the red line corresponds to graphene, and the others indicate PMMA residue.

current−voltage (I_D−V_G, I_D is the drain current and V_G is the gate voltage) characteristics of the GFETs in a vacuum (<10^{-6} Torr). It shows typical I_D−V_G curves with a large positive shift in the Dirac point, indicating that the graphene is highly p-doped even in vacuum. The GFETs had different performance depending on the initial concentration of PMMA solutions, and the Dirac point of each of the GFETs from the lowest concentration PMMA (10 mg/mL) were nearer to 0 V and the conductivity was higher (less p-type doping and higher room-temperature carrier mobility). When the devices were measured in ambient, the trend was the same as in vacuum, but the Dirac point was shifted more positively and the conductivity decreased.

The hole and electron mobility of each device was calculated using a diffusive transport model based on the total device resistance according to the following equation:[30,31]

$$R_{total} = R_{contact} + \frac{L}{We\mu\sqrt{n_o^2 + n[V_G^*]^2}} \quad (1)$$

where e is the elementary charge, μ is the field-effect mobility, n_o is the density of carriers at the Dirac point, and $n[V_G^*]$ is the value of the carrier concentration induced by the gate bias away from the Dirac point. By fitting this model to the measured I_D−V_G data, carrier mobilities were extracted with consideration of the contact resistance in our two-probe measurements. The calculated hole and electron mobilities measured in vacuum and air are shown in Figure 1c and d. The average hole (electron) mobilities for 12 GFET devices fabricated with PMMA solutions of 10, 40, and 80 mg/mL were 4280 ± 1050 (2500 ± 610), 2240 ± 430 (1670 ± 340), and 1720 ± 600 (1530 ± 590) cm^2/(V·s), respectively, in vacuum, and the average Dirac point voltages were 11.0 ± 3.7, 20.7 ± 12.4, and 36.3 ± 10.8 V, respectively. The hole (electron) mobilities in air were 2620 ± 920 (1910 ± 460), 1610 ± 300 (1100 ± 170), and 910 ± 300 (620 ± 360) cm^2/(V·s), respectively, and the Dirac point was shifted to 24.7 ± 4.5, 32.8 ± 4.5, and 52.7 ± 14.0 V, respectively. The data show that, when GFETs were fabricated with lower PMMA concentration solutions, less p-type doping and higher room-temperature carrier mobility were obtained. Also, Raman spectra (488 nm excitation laser with a 100× objective lens; WITec Alpha 300 micro-Raman imaging system) of the graphene films transferred using 80 mg/mL versus using 10 mg/mL PMMA showed that the graphene transferred by 10 mg/mL PMMA was less p-doped (Figure S1 in the Supporting Information: red shift of the G (2D) peak from 1587 (2702) to 1583 (2696) cm^{-1}, and the increase of the

I_{2D}/I_G from 1.74 to 3.04 for 80 mg/mL to 10 mg/mL PMMA).[32,33]

The p-type doping of graphene on SiO$_2$ has been explained in terms of several suggested mechanisms including charge transfer doping from H$_2$O/O$_2$ molecules,[13] an increase of external scattering sites due to polymer residue,[8,16] and metal contact effects.[34] The effect of charged impurities trapped between the graphene and SiO$_2$[10,35] can be ruled out in our study since the only experimental variable was the concentration of the polymer solution. It has been found that, for the p-doped graphene, the hole conduction is preserved while the electron conduction is suppressed as observed in our measurements.[36] The electron−hole asymmetry and sublinearity of the graphene conductance might be attributed in part to transport properties at the interface between graphene and metal contacts.[34] It has also been reported that metal contacts crossing whole graphene samples can induce those undesired characteristics.[37] However, doping with the metal contact is not the case for the changes of electrical properties as a function of the polymer solution concentrations in our experiments since all devices were fabricated at the same time. In our measurements, graphene was first transferred on SiO$_2$/Si by the polymer, and then metal electrodes were deposited. Thus, the polymer residue left between graphene and metal contacts might induce the changes of electrical properties of GFETs as a function of the initial concentrations of the PMMA solution. To clarify this question, GFETs were fabricated with bottom contact geometry; the metal electrodes were first deposited on SiO$_2$/Si, and graphene was transferred on it. As shown in Figure S2 (the Supporting Information), even for the GFETs having bottom contacts, the use of lower PMMA concentration solutions resulted in less p-type doping and higher carrier mobility. As a result, the effect of the concentration of PMMA solutions on electrical properties of GFETs does not originate from the metal contacts.

Since the electrical conductivity of graphene in vacuum was reduced as the concentration of PMMA solution was increased (in the range studied), the amount of PMMA residue on graphene seems to depend on the concentration of PMMA in chlorobenzene. As mentioned, when the GFETs were exposed to air the devices were more p-doped, and the trend of I_D−V_G curves in terms of concentration paralleled the trend in vacuum. This implies that the amount of H$_2$O/O$_2$ molecules that can be adsorbed in the PMMA residue and induce p-type doping varies with the initial concentration of the polymer solution. To further examine the amount of PMMA residue on graphene, XPS (Kratos AXIS Ultra DLD spectrometer, monochromated Al Kα emission at 1486.6 eV with an operating power of 150

W) data were obtained from monolayer graphene transferred onto SiO_2/Si. Figure 2 shows the C 1s core-level spectra of the different graphene samples. The C 1s background signals were subtracted by using the Shirley background model in the peak fitting. The sp^2 component of C—C bonding corresponding to graphene was modeled using the asymmetric Doniach—Sunjic line shape[38] and assigned to the binding energy of 284.4 eV.[39,40] Other spectral components fitted by a Gaussian/Lorentzian product formula corresponded to the different carbon species in PMMA: for example, C—H at 285.0 eV, C—C at 286.0 eV, C—O at 287.1 eV, and O—C=O at 289.1 eV.[16] The PMMA solution with lower concentrations yielded (relatively) smaller intensity for the C 1s peaks attributed to PMMA, indicating less PMMA residue on graphene.

An increase in the amount of PMMA residue for higher concentration PMMA solutions was measured with noncontact AFM (PSIA, model XE-1000S, Figure S3 of the Supporting Information). All graphene samples transferred with the different PMMA solutions used had 1−2 nm thick layers of the polymer, but the 80 mg/mL PMMA solution generated particularly large "polymer humps" on graphene (Figure S3a−c; i.e., the PMMA film was not uniform thickness). The two-dimensional power spectral density (2D-PSD) from the scanned area was calculated to compare the surface roughness of each sample (Figure S3d). The 2D-PSD provides information about surface roughness over different spatial frequency ranges and is used for understanding correlations between roughness and specific surface features.[41,42] The 2D-PSD spectra of the transferred graphene indicate that the graphene transferred using lower concentration PMMA has smoother surfaces over the whole spatial frequency range.

We thus speculate that, in a concentrated PMMA solution, the interactions among long polymer chains are stronger since the chains are more highly overlapped, which causes the polymer chains to become more entangled. Entanglement occurs where the polymer chains start to overlap.[43] We propose that the entangled polymer chains are not readily removed by conventional solvents when such a polymer solution is coated on graphene, yielding increased polymer residue including the larger polymer humps on the graphene surfaces that dope the graphene more p-type.

In an attempt to improve the electrical properties of graphene, the GFETs were treated with formamide. First, the graphene was transferred using a 10 mg/mL PMMA solution that was then "removed" by the typical acetone process. After the electrodes were deposited, the GFETs were simply dipped into a bath of formamide (ACS reagent grade, ≥99.5%, Sigma-Aldrich) overnight, and then the devices were blown with dry nitrogen. Figure 3 shows representative I_D-V_G curves of a GFET before and right after the formamide treatment. The Dirac point of this GFET shifted from 19.0 to 3.0 V in air after treatment. The hole (electron) mobility increased from 6800 (5650) to 10980 (10490) $cm^2/(V \cdot s)$. We measured eight devices before and after exposure to formamide. The average Dirac point voltage decreased from 27.0 ± 3.9 V to 2.7 ± 1.0 V in air. The average room-temperature hole (electron) mobility increased from 5120 ± 1150 (4740 ± 760) $cm^2/(V \cdot s)$ to 9850 ± 870 (9210 ± 820) $cm^2/(V \cdot s)$. All devices had more than a 50% improvement in room-temperature carrier mobility in air.

The significant enhancement of the electrical properties of graphene after the formamide treatment could be due to a rearrangement of the PMMA residue during the solvent treatment. Noncontact AFM was used to observe the
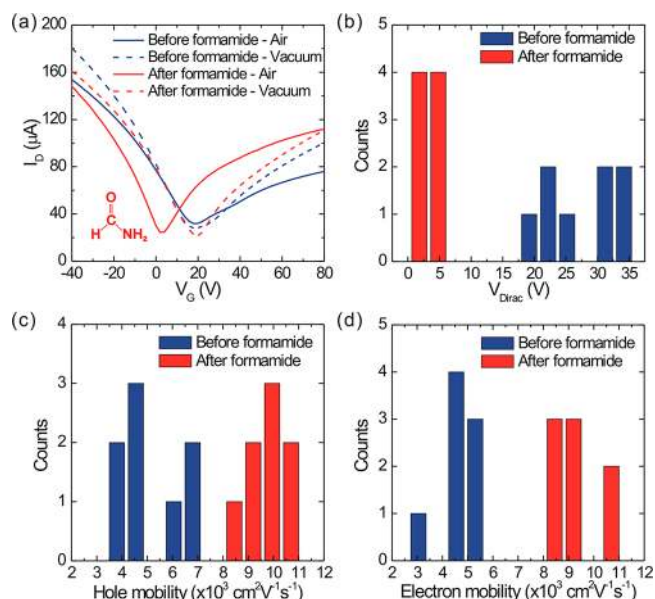
Figure 3. (a) Current−voltage (I_D-V_G) curves for the GFET measured in air and vacuum before and after the formamide treatment. The inset figure shows the chemical structure of formamide. (b−d) The Dirac point voltage and hole/electron mobilities for eight GFETs measured in air before and after the formamide treatment.

morphology of the polymer residue before and after the formamide treatment and as shown in Figure S4 (Supporting Information), the morphology of the graphene surface is similar after the treatment. Thus, rearrangement of the polymer residue is probably not occurring. Raman spectroscopy and XPS were used to further investigate the effects of formamide on graphene. For the graphene transferred with an 80 mg/mL PMMA solution, a significant red shift of the G (2D) peak from 1587 (2702) cm^{-1} to 1582 (2697) cm^{-1} and an increase of I_{2D}/I_G from 1.7 to 2.8 after the formamide treatment (Figure 4a) was observed by Raman spectroscopy. Figure 4b shows changes of the I_{2D}/I_G ratio and the G peak position of graphene transferred using 10 mg/mL or 80 mg/mL PMMA solutions before and after the formamide treatment. Although the graphene transferred with 80 mg/mL PMMA showed more recovery from the p-doping after the treatment, it was not better than that of the graphene transferred by 10 mg/mL PMMA before the treatment. XPS was done for graphene transferred using 10 mg/mL or 80 mg/mL PMMA. As shown in Figure 4c, after the formamide treatment, the N 1s spectrum had a peak for N in the amine group, suggesting that formamide is present on the transferred graphene. The (relative) peak intensity increased for the graphene transferred with 80 mg/mL PMMA compared to the graphene transferred with 10 mg/mL PMMA. It is likely that some of the formamide is solvated in the PMMA residue.

It has been reported that aminopropyltriethoxysilane or polyethylene imine molecules provide efficient n-type doping on carbon nanotubes through electron donation by the amine groups.[44,45] Recently, aminopropyltriethoxysilane deposited beneath monolayer graphene of back-gated FETs yielded n-type doping of the graphene channel; the amine group of the self-assembled monolayer reportedly donates its lone pair to graphene, which increases the electron carrier density and induces n-type doping.[46] In this respect, the amine group of formamide solvated in the thin PMMA layer likely donates

D

dx.doi.org/10.1021/nl304420b | Nano Lett. XXXX, XXX, XXX−XXX
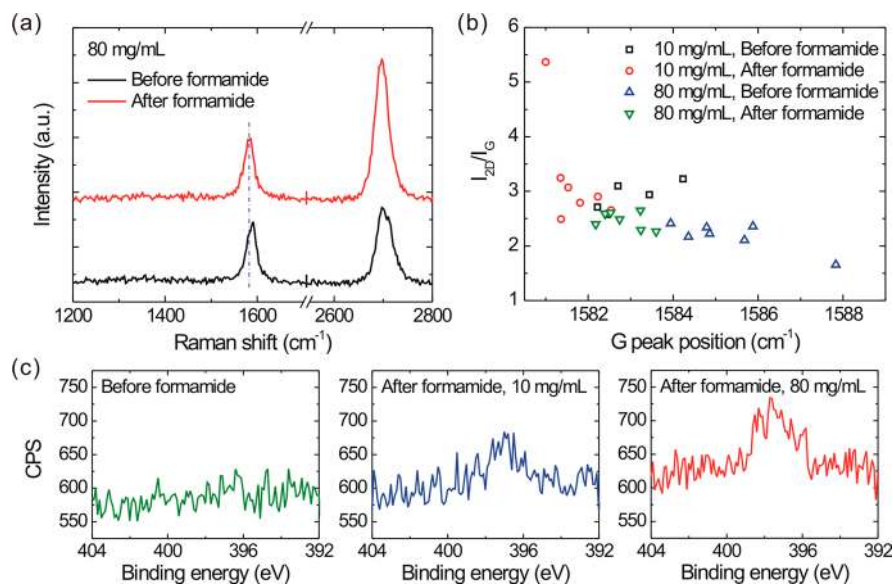
Figure 4. (a) Raman spectra of graphene transferred using 80 mg/mL PMMA before and after the formamide treatment. The blue-dashed line represents the G peak position of graphene after the formamide treatment. (b) I_{2D}/I_G versus G peak position of graphene films transferred by 10 mg/mL and 80 mg/mL PMMA. (c) XPS N 1s spectra of graphene before and after the formamide treatment.

electron charge at the interface with graphene. This charge compensates the p-type doping to restore the intrinsic electrical properties of the transferred CVD-grown graphene and as mentioned results in improved charge carrier mobility in air. However, when the formamide-treated GFET was placed in vacuum, the Dirac point shifted to the position for the untreated GFET in vacuum, and its carrier mobility decreased (Figure 3a). The hole (electron) mobility and the Dirac point of the formamide-treated GFET in vacuum are 7540 (7260) cm^2/(V·s) and 19.0 V, respectively, while the hole (electron) mobility and the Dirac point of the untreated GFET in vacuum are 6890 (4960) cm^2/(V·s) and 19.0 V, respectively. This might be due to the evaporation of formamide solvated in PMMA, showing p-type doping originated from PMMA residue. The restoration of the improved electrical properties of formamide-treated GFETs is much slower in air. The carrier mobility of the treated GFETs did not decrease much over several days, while the Dirac point moved back to the state before the treatment within several hours (Figure S6 in the Supporting Information). When the formamide slowly evaporated from PMMA in air, H_2O/O_2 also can be solvated in PMMA. The small amount of H_2O/O_2 might induce the significant shift of the Dirac point, while the carrier mobility was not affected much. A more detailed study for this phenomenon is needed for understanding the kinetic process of the evaporation of formamide solvated in PMMA.

The polymer residue can thus be used to modulate the electrical properties of graphene through the addition of other molecules. A previous work has shown that ammonia molecules can be sensed electrically by graphene having PMMA residue, but little electrical response to ammonia was obtained after the residue was largely removed.[19] Since the PMMA residue acts to solvate both formamide and H_2O/O_2 molecules, there would seem to be a competition between n-type doping from formamide residue and p-type doping from PMMA residues along with H_2O/O_2 molecules. Higher concentrations of PMMA leave more PMMA residue on graphene after its removal by acetone. Thus, it can also absorb more formamide, as confirmed by XPS. However, since this PMMA residue still

absorbs H_2O/O_2 molecules causing the graphene to become more p-doped by the electron transfer reaction involving the H_2O/O_2 redox couple,[13] the formamide-treated graphene transferred by higher concentrations of PMMA cannot surpass the electrical properties of the graphene transferred by the lower concentration of PMMA without formamide treatment, as shown by Raman spectroscopy (Figure 4b). This suggests that the combination of minimizing polymer residue and including an amine-based solvent treatment can provide the intrinsic electrical properties of CVD-grown graphene.

In summary, our work demonstrates the importance of polymer preparation and its impact on the electrical and surface characterization of graphene. Spin-coating of more concentrated polymer solutions can induce broad variations of electrical properties of CVD-grown graphene due to different amounts of polymer residue that remains as a thin and uneven film. Initially p-doped graphene (from a thin PMMA film) could be compensated by formamide solvated in the PMMA residue. This study thus also reveals the potential of deliberately using a polymer layer to control or recover the electrical properties of graphene.

■ ASSOCIATED CONTENT

Ⓢ Supporting Information

Details about experiments and analysis. This material is available free of charge via the Internet at http://pubs.acs.org.

■ AUTHOR INFORMATION

Corresponding Author

*E-mail: r.ruoff@mail.utexas.edu.

Notes

The authors declare no competing financial interest.

■ ACKNOWLEDGMENTS

■ REFERENCES

(1) Novoselov, K. S.; Geim, A. K.; Morozov, S. V.; Jiang, D.; Zhang, Y.; Dubonos, S. V.; Grigorieva, I. V.; Firsov, A. A. *Science* **2004**, *306* (5696), 666−669.

(2) Zhang, Y. B.; Tan, Y. W.; Stormer, H. L.; Kim, P. *Nature* **2005**, *438* (7065), 201−204.

(3) Lin, Y. M.; Dimitrakopoulos, C.; Jenkins, K. A.; Farmer, D. B.; Chiu, H. Y.; Grill, A.; Avouris, P. *Science* **2010**, *327* (5966), 662−662.

(4) Zhu, Y. W.; Murali, S.; Cai, W. W.; Li, X. S.; Suk, J. W.; Potts, J. R.; Ruoff, R. S. *Adv. Mater.* **2010**, *22* (35), 3906−3924.

(5) Li, X. S.; Cai, W. W.; An, J. H.; Kim, S.; Nah, J.; Yang, D. X.; Piner, R.; Velamakanni, A.; Jung, I.; Tutuc, E.; Banerjee, S. K.; Colombo, L.; Ruoff, R. S. *Science* **2009**, *324* (5932), 1312−1314.

(6) Li, X. S.; Zhu, Y. W.; Cai, W. W.; Borysiak, M.; Han, B. Y.; Chen, D.; Piner, R. D.; Colombo, L.; Ruoff, R. S. *Nano Lett.* **2009**, *9* (12), 4359−4363.

(7) Suk, J. W.; Kitt, A.; Magnuson, C. W.; Hao, Y. F.; Ahmed, S.; An, J. H.; Swan, A. K.; Goldberg, B. B.; Ruoff, R. S. *ACS Nano* **2011**, *5* (9), 6916−6924.

(8) Ishigami, M.; Chen, J. H.; Cullen, W. G.; Fuhrer, M. S.; Williams, E. D. *Nano Lett.* **2007**, *7* (6), 1643−1648.

(9) Schedin, F.; Geim, A. K.; Morozov, S. V.; Hill, E. W.; Blake, P.; Katsnelson, M. I.; Novoselov, K. S. *Nat. Mater.* **2007**, *6* (9), 652−655.

(10) Chen, J. H.; Jang, C.; Xiao, S. D.; Ishigami, M.; Fuhrer, M. S. *Nat. Nanotechnol.* **2008**, *3* (4), 206−209.

(11) Chen, J. H.; Jang, C.; Adam, S.; Fuhrer, M. S.; Williams, E. D.; Ishigami, M. *Nat. Phys.* **2008**, *4* (5), 377−381.

(12) Ryu, S.; Liu, L.; Berciaud, S.; Yu, Y. J.; Liu, H. T.; Kim, P.; Flynn, G. W.; Brus, L. E. *Nano Lett.* **2010**, *10* (12), 4944−4951.

(13) Levesque, P. L.; Sabri, S. S.; Aguirre, C. M.; Guillemette, J.; Siaj, M.; Desjardins, P.; Szkopek, T.; Martel, R. *Nano Lett.* **2011**, *11* (1), 132−137.

(14) Cheng, Z. G.; Zhou, Q. Y.; Wang, C. X.; Li, Q. A.; Wang, C.; Fang, Y. *Nano Lett.* **2011**, *11* (2), 767−771.

(15) Pettes, M. T.; Jo, I. S.; Yao, Z.; Shi, L. *Nano Lett.* **2011**, *11* (3), 1195−1200.

(16) Pirkle, A.; Chan, J.; Venugopal, A.; Hinojos, D.; Magnuson, C. W.; McDonnell, S.; Colombo, L.; Vogel, E. M.; Ruoff, R. S.; Wallace, R. M. *Appl. Phys. Lett.* **2011**, *99* (12), 122108.

(17) Li, X. S.; Magnuson, C. W.; Venugopal, A.; An, J. H.; Suk, J. W.; Han, B. Y.; Borysiak, M.; Cai, W. W.; Velamakanni, A.; Zhu, Y. W.; Fu, L. F.; Vogel, E. M.; Voelkl, E.; Colombo, L.; Ruoff, R. S. *Nano Lett.* **2010**, *10* (11), 4328−4334.

(18) Song, H. S.; Li, S. L.; Miyazaki, H.; Sato, S.; Hayashi, K.; Yamada, A.; Yokoyama, N.; Tsukagoshi, K. *Sci. Rep.* **2012**, *2*, 337.

(19) Dan, Y. P.; Lu, Y.; Kybert, N. J.; Luo, Z. T.; Johnson, A. T. C. *Nano Lett.* **2009**, *9* (4), 1472−1475.

(20) Lin, Y. C.; Lu, C. C.; Yeh, C. H.; Jin, C. H.; Suenaga, K.; Chiu, P. W. *Nano Lett.* **2012**, *12* (1), 414−419.

(21) Ni, Z. H.; Wang, H. M.; Ma, Y.; Kasim, J.; Wu, Y. H.; Shen, Z. X. *ACS Nano* **2008**, *2* (5), 1033−1039.

(22) Ni, Z. H.; Wang, H. M.; Luo, Z. Q.; Wang, Y. Y.; Yu, T.; Wu, Y. H.; Shen, Z. X. *J. Raman Spectrosc.* **2010**, *41* (5), 479−483.

(23) Lee, W. H.; Suk, J. W.; Lee, J.; Hao, Y. F.; Park, J.; Yang, J. W.; Ha, H. W.; Murali, S.; Chou, H.; Akinwande, D.; Kim, K. S.; Ruoff, R. S. *ACS Nano* **2012**, *6* (2), 1284−1290.

(24) Lee, J.; Tao, L.; Hao, Y.; Ruoff, R. S.; Akinwande, D. *Appl. Phys. Lett.* **2012**, *100* (15), 152104.

(25) Lee, E.; Lee, K.; Liu, C. H.; Kulkarni, G. S.; Zhong, Z. H. *Nat. Commun.* **2012**, *3*, 1018.

(26) Lee, S. K.; Jang, H. Y.; Jang, S.; Choi, E.; Hong, B. H.; Lee, J.; Park, S.; Ahn, J. H. *Nano Lett.* **2012**, *12* (7), 3472−3476.

(27) Tao, L.; Lee, J.; Akinwande, D. *J. Vac. Sci. Technol., B* **2011**, *29* (6), 06FG07.

(28) Lu, C. C.; Lin, Y. C.; Yeh, C. H.; Huang, J. C.; Chiu, P. W. *ACS Nano* **2012**, *6* (5), 4469−4474.

(29) Moser, J.; Barreiro, A.; Bachtold, A. *Appl. Phys. Lett.* **2007**, *91* (16), 163513.

(30) Kim, S.; Nah, J.; Jo, I.; Shahrjerdi, D.; Colombo, L.; Yao, Z.; Tutuc, E.; Banerjee, S. K. *Appl. Phys. Lett.* **2009**, *94* (6), 062107.

(31) Ha, T. J.; Akinwande, D.; Dodabalapur, A. *Appl. Phys. Lett.* **2012**, *101* (3), 033309.

(32) Das, A.; Pisana, S.; Chakraborty, B.; Piscanec, S.; Saha, S. K.; Waghmare, U. V.; Novoselov, K. S.; Krishnamurthy, H. R.; Geim, A. K.; Ferrari, A. C.; Sood, A. K. *Nat. Nanotechnol.* **2008**, *3* (4), 210−215.

(33) Casiraghi, C. *Phys. Rev. B* **2009**, *80* (23), 233407.

(34) Giovannetti, G.; Khomyakov, P. A.; Brocks, G.; Karpan, V. M.; van den Brink, J.; Kelly, P. J. *Phys. Rev. Lett.* **2008**, *101* (2), 026803.

(35) Adam, S.; Hwang, E. H.; Galitski, V. M.; Das Sarma, S. *Proc. Natl. Acad. Sci. U.S.A.* **2007**, *104* (47), 18392−18397.

(36) Farmer, D. B.; Golizadeh-Mojarad, R.; Perebeinos, V.; Lin, Y. M.; Tulevski, G. S.; Tsang, J. C.; Avouris, P. *Nano Lett.* **2009**, *9* (1), 388−392.

(37) Huard, B.; Stander, N.; Sulpizio, J. A.; Goldhaber-Gordon, D. *Phys. Rev. B* **2008**, *78* (12), 121402(R).

(38) Doniach, S.; Sunjic, M. *J. Phys., Part C: Solid* **1970**, *3* (2), 285−291.

(39) Suk, J. W.; Murali, S.; An, J.; Ruoff, R. S. *Carbon* **2012**, *50* (6), 2220−2225.

(40) Some, S.; Kim, Y.; Hwang, E.; Yoo, H.; Lee, H. *Chem. Commun.* **2012**, *48* (62), 7732−7734.

(41) Sawant, P. D.; Sabri, Y. M.; Ippolito, S. J.; Bansal, V.; Bhargava, S. K. *Phys. Chem. Chem. Phys.* **2009**, *11* (14), 2374−2378.

(42) Boyard, N.; Serre, C.; Vayer, M. *J. Appl. Polym. Sci.* **2007**, *103* (1), 451−461.

(43) Colby, R. H.; Fetters, L. J.; Funk, W. G.; Graessley, W. W. *Macromolecules* **1991**, *24* (13), 3873−3882.

(44) Shim, M.; Javey, A.; Kam, N. W. S.; Dai, H. J. *J. Am. Chem. Soc.* **2001**, *123* (46), 11512−11513.

(45) Kong, J.; Dai, H. J. *J. Phys. Chem. B* **2001**, *105* (15), 2890−2893.

(46) Yan, Z.; Sun, Z. Z.; Lu, W.; Yao, J.; Zhu, Y.; Tour, J. M. *ACS Nano* **2011**, *5* (2), 1535−1540.